JPE 16-6-33

http://dx.doi.org/10.6113/JPE.2016.16.6.2338
ISSN(Print): 1598-2092 / ISSN(Online): 2093-4718

Impedance Matching Based Control for the Resonance Damping of Microgrids with Multiple Grid Connected Converters

Shulong Tan†, Hua Geng*, and Geng Yang*

†,*Department of Automation, Tsinghua University, Beijing, China

Abstract

This paper presents an impedance-matching-based control scheme for the harmonic resonance damping of multiple grid-connected-converters (GCCs) with *LCL* filters. As indicated in this paper, harmonic resonance occurs if a GCC possesses an output impedance that is not matched with the rest of the network in some specific frequency bands. It is also revealed that the resonance frequency is associated with the number of GCCs, the grid impedance and even the capacitive loads. By controlling the grid-side current instead of the converter-side current, the critical *LCL* filter is restricted as an internal component. Thus, the closed-loop output impedance of the GCC within the filter can be configured. The proposed scheme actively regulates the output impedance of the GCC to match the impedance of the external network, based on the detected resonance frequency. As a result, the resonance risk of multiple GCCs can be avoided, which is beneficial for the plug-and-play property of the GCCs in microgrids. Simulation and experimental results validate the effectiveness of the proposed method.

Key words: Grid-connected-converters, Impedance matching, LCL filter, Resonance damping

I. INTRODUCTION

More and more distributed generation (DG) units have been integrated into low-voltage (LV) distribution systems in recent years [1], [2]. As an efficient form to achieve the coordinated operation of DG units in certain application, the microgrid is gradually gaining wide acceptance [3]. In spite of its high efficiency and control flexibilities [4], the microgrid still faces new technical challenges. In a microgrid, grid-connected-converters (GCCs) with *LCL* filters are widely applied as a power interface between the DGs and the distribution system [5]. *LCL* resonance can be excited by system harmonics either from the PWM process or from grid voltage distortions [6]. Moreover, this can be intensified by other paralleled GCCs with their own resonances [7], [8]. Resonance in a microgrid leads to line current distortions or even harmonic instability of the whole system [8].

To suppress the harmonic resonance of GCCs with *LCL* filters, some active damping control methods have been proposed. The basic idea is to introduce system state variables to achieve feedback control [9]. Examples of these state variables include the filter capacitor voltage [10], [11], the inverter-side inductor current [12], and the filter capacitor current [13]-[16]. Moreover, multiple-state feedback is also employed for active damping [17]. Among the various solutions in these studies, the double-loop grid-side current control based on filter capacitor current feedback is generally preferred [18].

Nevertheless, these approaches mainly address the resonance suppression of individual GCCs. Once more GCCs are connected to a network, new resonance problems may occur [19]. It is indicated in [7], [19], and [20] that the interaction of multiple GCCs is likely to result in parallel resonance among the GCCs. Simultaneously, series resonance also occurs between a multiple-GCC-based system and a distribution grid. Given the complex resonances of multiple GCCs in a microgrid, a few papers have been published to address this issue. An active damper was developed in [21] to reshape the external impedance profile of the GCCs, so as to prevent the resonance between the external network and the GCCs. An impedance converter was

Manuscript received May 18, 2016; accepted Aug. 10, 2016
Recommended for publication by Associate Editor Jae-Do Park.
†Corresponding Author: tansl_mail@foxmail.com
Tel: +86-18811360602, Tsinghua University
*Department of Automation, Tsinghua University, China

proposed in [22] to eliminate the reflected wave and damp the background harmonic resonance in the grid. These methods implement a special "stabilizer" to effectively handle the resonance in a microgrid from the perspective of the external network. Another option is to deal with the resonance from the perspective of the GCC itself. A lead-lag element is used in the control scheme of each GCC to damp oscillations in an *n*-paralleled GCCs system [19]. A virtual-impedance-based active damping method is adopted for each of the GCCs in a microgrid [7]. However, the authors of this paper just consider the regulation of the current coming from the converter, rather than the current injecting into the grid after a *LCL* filter. Therefore, the *LCL* filter is susceptible to coupling with an external network as an intermediate component without constraints by the current control loop, which may pose a potential threat to system stability. In addition, the performance of these methods, which were designed with a relatively fixed parameter, may degrade because the structure and impedance characteristics of the external network which the GCC is confronted with will be variable and complicated as the microgrid is further developed [4], [23], [24]. In order to deal with the harmonic resonance in increasingly complicated microgrids, it is necessary to take a comprehensive consideration of the GCC, the coupling among multiple GCCs, the grid impedance, the special distributed, etc. Then it is necessary to explore the causes of the resonance and the corresponding solution from the perspective of the system level.

As mentioned above, an external network of GCCs will present mutative impedance characteristics in different frequency bands under a variety of conditions. Thus, it is possible to generate the resonance mode together with the output impedances of the GCCs. This situation is called "impedance mismatch" in this paper. By targeting the grid-side current directly, this paper presents an impedance-matching-based GCC control scheme for resonance damping. Since the critical *LCL* filter is restrained as an internal component, the closed-loop output impedance of a GCC with a filter as a whole can be configured to match the impedance of the external network, based on the detected resonance frequency. Consequently, the harmonic resonance in microgrids is dampened.

II. Modeling and Stability Analysis

A. System Description

Fig. 1 shows a three-phase grid interactive microgrid comprised of *n* parallel DG systems and linear loads. The grid impedance is denoted by R_g and L_g. The traditional resistor-inductance load is described as R_L and L_L. The generalized capacitive loads are represented by C_L, for example the power electronics equipment installed for reactive power output. Each DG system is connected to the grid at the point of common coupling (PCC) through a *LCL* filter. For the *LCL* filter, L_1 is the inverter-side inductance, L_2 is the grid-side inductance, and C_f is the filter capacitance. The DC bus voltage of the DG system is assumed to be a constant for the sake of the resonance investigation. It is also assumed that the three-phase system is balanced. In addition, the switching frequency of the GCC is sufficiently high in this investigation. Therefore, its effect on the control dynamics can be neglected. Under the above assumptions, the GCC system can be represented by a linearized "average switching model (ASM)" [25].

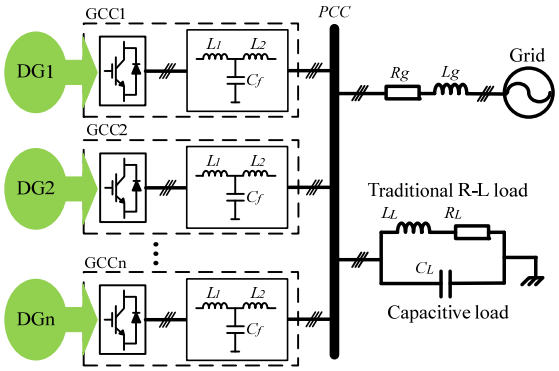

Fig. 1. Configuration of a multiple-GCC-based microgrid.

B. Conventional Control of GCCs with a LCL Filter

In a microgrid, each GCC is regulated by a preferred double-loop control scheme [14], [18], as shown in Fig. 2. The equivalent single-phase ASM is presented in Fig. 3, where the grid-side current i_g is set as the control object, and the filter capacitor current i_C is measured to stabilize the system and to dampen the resonance. i_g^* represents the current reference. The inverter-side current is denoted by i_1, and the filter capacitor voltage is expressed by u_C. u_{inv} is the output voltage of the inverter, and u_{PCC} is used for system synchronization. The proportional gain of the inner feedback loop for the capacitor current is k_{ic}. The outer loop in Fig. 3 is a general transfer function represented by $C(s)$. In this investigation, it is implemented as a proportional resonant (PR) controller, which is equally applicable to single or three phase systems.

The PR controller transfer function, given by (1), has an infinite gain at the fundamental frequency. Therefore, it can eliminate the steady state error.

$$C(s) = k_p + \frac{k_r s}{s^2 + \omega_0^2} \tag{1}$$

According to the control block diagram of the GCC, its closed-loop behavior acts as a double input and single output system, as shown in (2).

$$i_g = G_c(s) i_g^* - \frac{1}{Z_c}(s) u_{PCC} \tag{2}$$

where $G_c(s)$ is the reference-to-output transfer function of the grid-side current, and $Z_c(s)$ represents the closed-loop output impedance of the GCC. Both of them largely depend on the

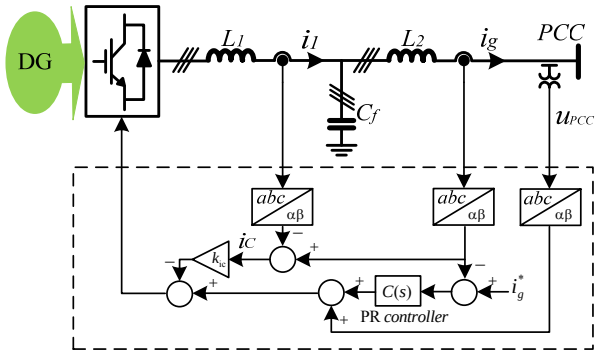

Fig. 2. Block diagram of conventional control for the GCC.

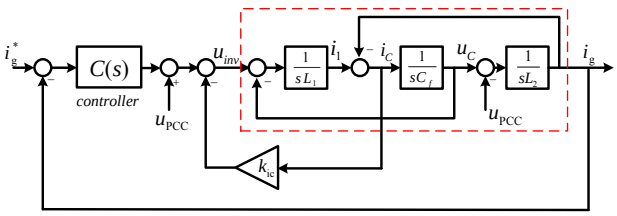

Fig. 3. Single-phase ASM of conventional control for the GCC.

control scheme of the GCC, as shown in (3) and (4).

$$G_c(s)=\frac{C(s)}{s^3L_1L_2C_f+s^2k_{ic}L_2C_f+s(L_1+L_2)+C(s)} \tag{3}$$

$$Z_c(s)=\frac{s^3L_1L_2C_f+s^2k_{ic}L_2C_f+s(L_1+L_2)+C(s)}{s^2L_1C_f+sk_{ic}C_f} \tag{4}$$

C. Closed-loop Norton Equivalent Circuit Model

After establishing a model of the single GCC system in (2), the closed-loop Norton equivalent circuit of a microgrid can be obtained in Fig. 4. Each GCC with the double-loop control scheme in Fig.1 is substituted by a controlled current source with a parallel output impedance. The grid voltage u_s is connected to the PCC with its series impedance. It is worth noting that the ordinary resistor-inductance loads are neglected, and the capacitive loads are lumped together with the grid impedance of the distribution system, denoted by the impedance $Z_{ext}(s)$, as shown in (5).

$$Z_{ext}(s)=\frac{sL_g+R_g}{s^2L_gC_L+sR_gC_L+1} \tag{5}$$

Based on the developed model, the grid currents of the GCCs can be derived. For the sake of simplicity, it is assumed that all of the GCCs in the microgrid have identical circuits and control parameters while the current reference for each GCC is independently generated. Taking the grid current of GCC1 as an example, it can be obtained as shown in (6), after a series of manipulations.

$$\begin{aligned} i_{g1}&=\frac{(n-1)Z_{ext}(s)+Z_c(s)}{nZ_{ext}(s)+Z_c(s)}G_c(s)i_{g1}^*-\cdots \\ &\cdots-\frac{1}{nZ_{ext}(s)+Z_c(s)}\left[Z_{ext}(s)G_c(s)(i_{g2}^*+\cdots+i_{gn}^*)+u_s\right] \end{aligned} \tag{6}$$

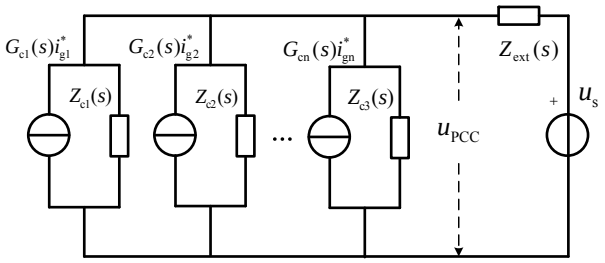

Fig. 4. Closed-loop Norton equivalent circuit of the microgrid.

D. Stability Analysis of a Microgrid

After further mathematical derivations, the grid current of GCC1 in a microgrid can be rearranged as follows:

$$\begin{aligned} i_{g1}&=\frac{1}{1+\dfrac{Z_{ext}(s)}{(n-1)Z_{ext}(s)+Z_c(s)}}G_c(s)i_{g1}^*-\cdots \\ &\cdots-\frac{1}{1+\dfrac{Z_c(s)}{nZ_{ext}(s)}}\frac{1}{n}\left[G_c(s)(i_{g2}^*+\cdots+i_{gn}^*)+\frac{1}{Z_{ext}(s)}u_s\right] \end{aligned} \tag{7}$$

It is reasonable to assume that the grid voltage is stable when unloaded and that the GCC is stable when connected to an ideal stiff grid. Thus, the stability of the grid currents depends on the following item $H_c(s)$, which is the multiplier of the first item in (7). Since the multiplier for the second item is found to be included in $H_c(s)$ by mathematical derivation, $H_c(s)$ can determine the stability of the system.

$$H_c(s)=\frac{1}{1+\dfrac{Z_{ext}(s)}{(n-1)Z_{ext}(s)+Z_c(s)}} \tag{8}$$

It is obvious that $H_c(s)$ resembles a close-loop transfer function of a negative feedback control system, where the forward gain is unity and the feedback gain is $T_c(s)$, as shown in (9).

$$T_c(s)=\frac{Z_{ext}(s)}{(n-1)Z_{ext}(s)+Z_c(s)} \tag{9}$$

According to linear control theory, the stability of the grid currents in a microgrid depends on whether $T_c(s)$ satisfies the Nyquist stability criterion [26]. It is revealed that the harmonic resonance resulting from the dynamic interactions between the GCC output impedance and the impedance of the external network, which includes the grid impedance and loads, is a special stability issue in multiple-GCC-based microgrids.

III. Investigation on the Resonances in Microgrids

As previously mentioned, the grid impedance, the capacitive loads, the amount of GCCs and the closed-loop output impedance of the GCCs may affect the stability of a microgrid. By illustrating the step by step derivation process of the stability criterion $T_c(s)$ in Bode diagrams, each factor can be investigated graphically in detail. A microgrid

consisting of three GCCs is taken as an example. All of the GCCs adopt the conventional double-loop control scheme shown in Fig. 2. The electrical constants and control parameters are listed in Table I. For the sake of simplicity, the outer loop controller $C(s)$ of the GCC is implemented as a proportional controller instead of a PR controller. This is due to the fact that resonant controllers are negligible in the harmonic-frequency region (typically from hundreds of Hz to several kHz) [8].

Fig. 5 shows a Bode diagram of the stability criterion $T_c(s)$ and its derivation process. The red dash curve represents the lumped external impedance $Z_{ext}(s)$, without capacitive loads in this case. The red solid curve is n-1 times of $Z_{ext}(s)$, which assist in calculating $T_c(s)$. The black dash curve represents the closed-loop output impedance of the GCC, namely $Z_c(s)$. According to (9), the stability criterion $T_c(s)$ can be derived as shown by the black solid curve. It is obvious that the sum of n-1 times of $Z_{ext}(s)$ and the output impedance $Z_c(s)$ becomes the denominator in (9), which is critical for the stability criterion $T_c(s)$. Taking Fig. 5 as an example, the amplitude-frequency curves of $Z_c(s)$ and n-1 times $Z_{ext}(s)$ intersect at a frequency around 600Hz, while their corresponding phase-frequency characteristics are almost opposite. As a result, their sum is nearly zero, which is the denominator of $T_c(s)$. Therefore, a peak occurs in the amplitude-frequency curve of the stability criterion at the corresponding frequency, and hence a resonance peak occurs in the closed-loop amplitude-frequency curve of $H_c(s)$. Since active damping of the conventional double-loop control scheme is implemented for each GCC, the stability of the whole microgrid system is still maintained. However, a resonance peak occurs on the closed-loop amplitude-frequency curve of the grid currents in the microgrid. Consequently, a sustained harmonic resonance is predictable at a frequency around 600Hz. As shown in Fig. 5, the output impedance of the GCC, namely $Z_c(s)$, is almost capacitive in the resonance frequency region where the peak of $T_c(s)$ is located. Meanwhile, the lumped external impedance $Z_{ext}(s)$ is inductive in the same region. It can be concluded that an impedance mismatch between the GCCs and the external network in some specific frequency bands is the cause of the resonance in the microgrid.

By a further analysis of the derivation in Fig. 5, it is found that the intersection in the amplitude-frequency curves of $Z_c(s)$ and n-1 times $Z_{ext}(s)$ shifts to a low-frequency region when the grid inductance or the number of parallel GCCs increases. Hence, the resonance frequency is expected to decrease. For the resonance analysis, the impact of the grid impedance variation and the impact of the amount variation of the parallel GCCs are analogous. As an illustration, the effect of grid impedance variation is shown in Fig. 6. When the grid inductance increases from 0.6mH to 2.6mH, the peak of the amplitude-frequency curve drifts to the low-frequency

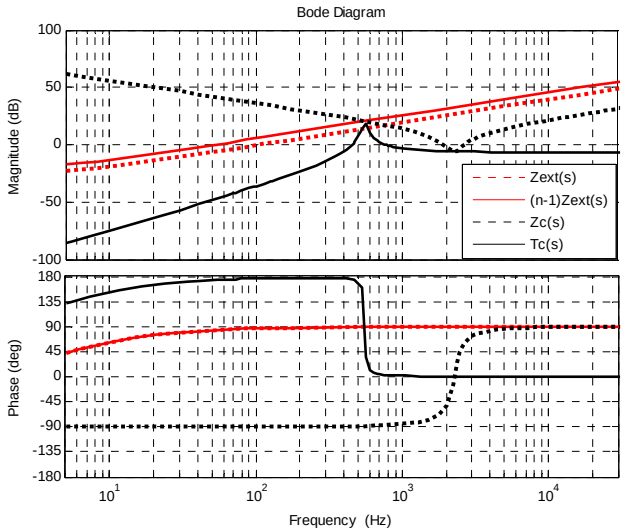

Fig. 5. Bode diagram of $T_c(s)$ without the capacitive load.

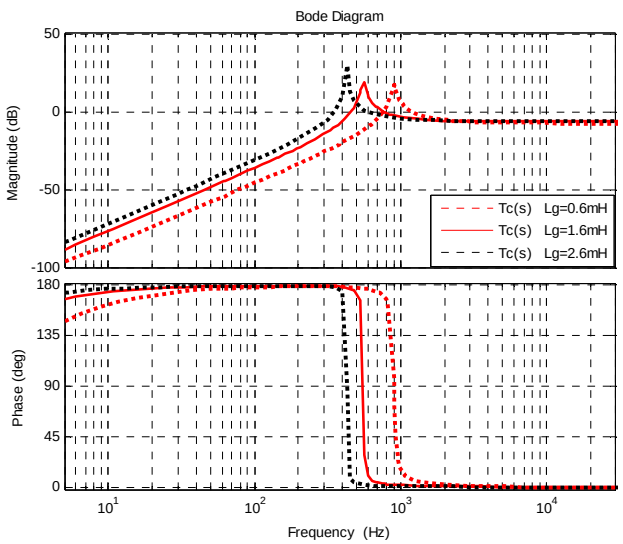

Fig. 6. Bode diagram of $T_c(s)$ with grid impedance variation.

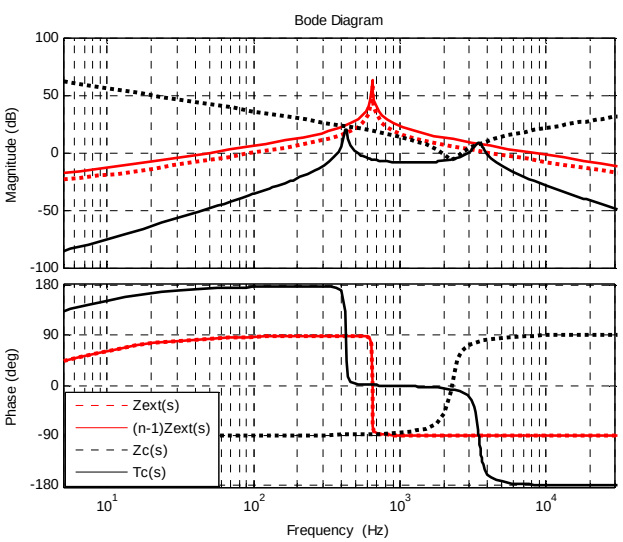

Fig. 7. Bode diagram of $T_c(s)$ with the capacitive load.

region. Meanwhile, the phase margin also gets narrow.

When the capacitive loads are taken into consideration, a Bode diagram of $T_c(s)$ and its derivation process are illustrated in Fig. 7. There is a peak in the amplitude-frequency curve of the lumped external impedance $Z_{ext}(s)$ due to the participation of the capacitive loads. Accordingly, the intersection in the amplitude-frequency curves of $Z_c(s)$ and n-1 times $Z_{ext}(s)$ moves a significant step towards the low-frequency region, compared with the one in Fig. 5. The resonance frequency is likely to be about 400Hz when the capacitive loads are switched in. In addition, a new peak appears in the amplitude-frequency curve of $T_c(s)$ in the high-frequency region. Since the corresponding stability margin is relatively large and the resonance attenuation in the high frequency region is more obvious, the new peak is insignificant in the resonance analysis.

IV. Proposed Impedance-Matching-Based Method

According to the aforementioned analysis, a method based on impedance matching is introduced to mitigate resonance. It employs a multi-loop control scheme for resonance damping, together with a PR controller to regulate the grid current. Unlike the conventional methods, this solution is proposed from the perspective of the whole microgrid instead of a single GCC. It takes into consideration the resonance frequency variation, which is affected by the number of GCCs, the grid impedance and the capacitive loads. Thus, the closed-loop output impedance of each GCC can be adjusted to match the impedance of the external network, based on the detected resonance frequency. In this section, an accurate equivalent circuit of this method is illustrated, the distinct physical meanings of the control parameters are demonstrated, and the performance of the resonance suppression is analyzed.

A. Principle of the Proposed Method

It is well known that the capacitor shunt branch of a *LCL* filter performs super-low impedance at high frequencies for the switching harmonic. However, by coupling with an external network in a microgrid, its capacitive character may lead to harmonic resonance in the harmonic-frequency region. Experimental investigations have demonstrated this phenomenon and a schematic diagram is shown in Fig. 8. The converter-side current contains a fundamental component and the switching harmonic. The switching harmonic is filtered out through the capacitor shunt branch as expected, and only the fundamental component is transmitted to the external power grid. Nevertheless, there is an adverse side effect to this. Harmonic resonance is found between the grid-side current and the capacitor current. It is introduced by the coupling between the capacitor shunt branch and the external

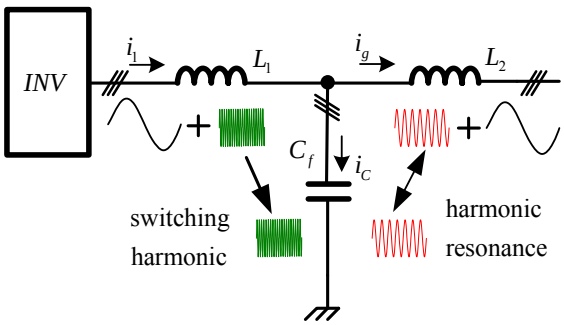

Fig. 8. Harmonic resonance in the capacitor shunt branch.

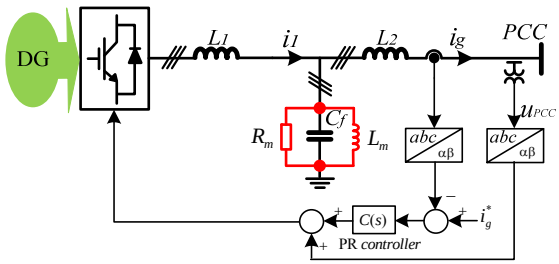

Fig. 9. Equivalent circuit of the proposed method.

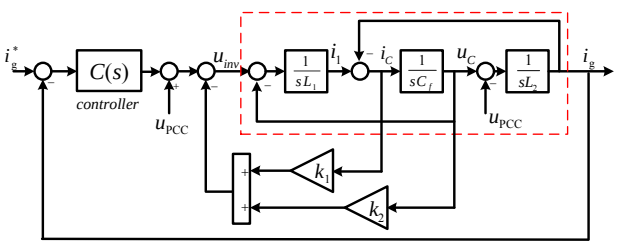

Fig. 10. Block diagram of the proposed method.

network which is mainly inductive in the resonance frequency region. Naturally, it seems reasonable to reconstruct the critical capacitor shunt branch according to the proposed control scheme to achieve impedance matching between the GCCs and the external network.

In order to achieve resistive impedance instead of capacitive impedance in the harmonic-frequency region, an equivalent inductor shunt branch is implemented by the proposed method, namely L_m in Fig. 9. When the resonant frequency of the branch, consisting of a filter capacitor and an equivalent inductor, is located at the harmonic-frequency, the corresponding phase of the closed-loop output impedance of the GCC, namely $Z_c(s)$, is about 0° instead of -90° in Fig. 5. Therefore, the critical inductance-capacitance mismatch between the external network and the GCCs is avoided. Meanwhile, the filtering performance at a much higher frequency for the switching harmonic is not compromised because of the frequency selectivity. Nevertheless, this situation is extremely sensitive to system parameters and prone to instability. Hence, an equivalent resistor shunt branch, R_m, is implemented for the sake of robustness.

Consequently, the expected resistive impedance region is expanded significantly, and the proposed method is immune

to parameter variations in a wide range.

According to the equivalent circuit of the proposed impedance-matching based control, the reconstructed output impedance of the GCC can be obtained in (10). Comparing the original output impedance in (4) with the conventional double-loop control scheme, the zero and pole placement of the output impedance can be reconfigured by the proposed method. This also means that the impedance characteristic of the GCCs in a specific frequency band can be configured to match with that of the external network.

$$Z_c(s)=\frac{s^3L_1L_2C_f+s^2\frac{1}{R_m}L_1L_2+s(L_1+L_2+\frac{1}{L_m}L_1L_2)+C(s)}{s^2L_1C_f+s\frac{L_1}{R_m}+\frac{L_1}{L_m}} \quad (10)$$

To achieve the equivalent inductor and resistor shown in Fig. 9, a multi-loop control scheme consisting of the feedback of the filter capacitor current i_C and filter capacitor voltage u_C is introduced. A block diagram of the equivalent single-phase ASM for the proposed method is illustrated in Fig. 10. The proportional gains of the inner feedback loops for the capacitor current and capacitor voltage are k_1 and k_2, respectively. Based on the control block diagram, the corresponding closed-loop output impedance of the GCC can also be derived, as expressed in (11).

$$Z_c(s)=\frac{s^3L_1L_2C+s^2k_1L_2C+s(L_1+L_2+k_2L_2)+C(s)}{s^2L_1C+sk_1C+k_2} \quad (11)$$

Comparing (11) with (10), the distinct physical meanings of the feedback parameters in Fig.10 can be obtained. The relationship between the equivalent circuit elements in Fig. 9 and the proportional gains of the inner feedback loops in Fig. 10 is represented in (12) and (13).

$$k_1=\frac{L_1}{R_mC_f} \quad (12)$$

$$k_2=\frac{L_1}{L_m} \quad (13)$$

As mentioned above, the resonant frequency of the branch consisting of a filter capacitor and an equivalent inductor is supposed to be located at the detected harmonic frequency, which is represented by f_{har}. The following relationship should be satisfied to ensure an approximate resistive impedance in the harmonic-frequency region.

$$f_{har}=\frac{1}{2\pi}\sqrt{L_mC_f} \quad (14)$$

Based on a previous analysis, it is found that an equivalent resistor shunt branch is also necessary to make the impedance configuration less sensitive to system parameter variations. In general, the equivalent resistor should be chosen according to the following requirement, as shown in (15).

$$R_m=\frac{1}{2\pi f_{har}C_f} \quad (15)$$

With (15) as the controller parameter, a minimal impact is exerted on the amplitude-frequency curve of the GCC output

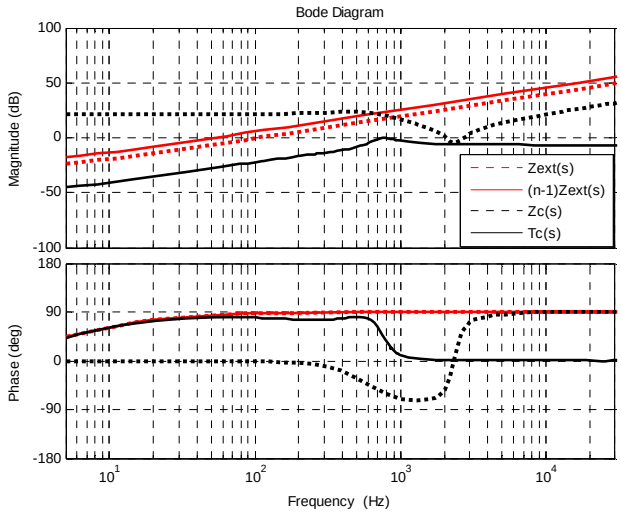

Fig. 11. Bode diagram of $T_c(s)$ when the capacitive load is off.

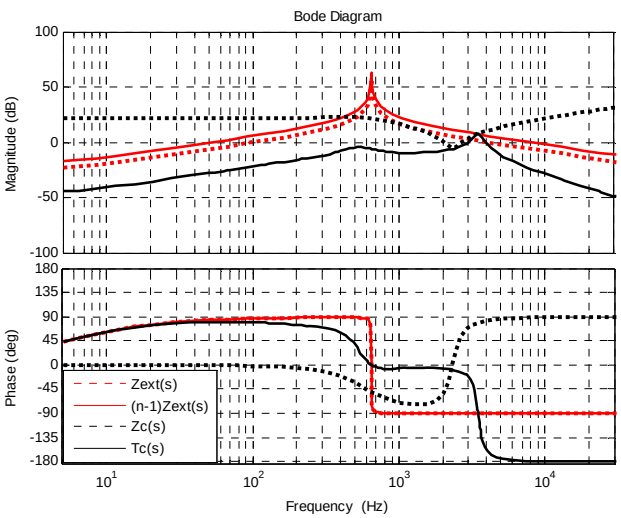

Fig. 12. Bode diagram of $T_c(s)$ when the capacitive load is on.

impedance around the harmonic frequency. Therefore, the location of the intersection in the amplitude-frequency curves is maintained and the corresponding phase is significantly reconstructed. Variations of the grid impedance, the number of GCCs and the loads are taken into consideration in the proposed method since they regulate the output impedance of the GCC based on the detected resonance frequency f_{har}. In addition, the parameter robustness introduced by the equivalent resistor also makes the proposed method less sensitive to the random variations of the output filter impedance of the GCC during operation.

Feedback loops of the filter capacitor current i_C and filter capacitor voltage u_C are clarified separately in Fig. 10. It seems that the proposed method needs more sensors. However, this will result in cost increases. In fact, the estimation of certain system states can reduce the spending in terms of required sensors. For example, the current sensors implemented in the feedback loop of the filter capacitor

TABLE I
ELECTRICAL CONSTANTS AND CONTROL PARAMETERS

Parameters	Symbols	Values
grid impedance	L_g, R_g	1.6mH, 0.1Ω
capacitive load	C_L	40uF
LCL filter parameter	L_1, C_f, L_2	3mH,20uF,0.2mH
grid voltage	U_s	200V
grid frequency	f_g	50Hz
DC link voltage	V_{dc}	450V
switching frequency	f_s	12.5kHz
PR control parameter	k_p, k_r	10, 3000
parameter of conventional control	k_{ic}	12
parameters of proposed control	k_1, k_2	12, 0.91

current can be omitted, since the derivation of the filter capacitor voltage is a simple method for estimating the filter capacitor current. Relevant theoretical derivation and experimental verification can be found in [13].

B. Mitigation of Resonance in the Microgrid

After the parameters of the proposed method are chosen, the effectiveness of the proposed method for the resonance suppression in a microgrid is examined by using a Bode diagram. In this investigation, the harmonic frequency f_{har} is chosen as 600Hz, as mentioned in Fig. 5, where a microgrid consisting of three GCCs is taken as a basic case. The electrical constants and control parameters are listed in Table I. As previously discussed, the outer loop controller $C(s)$ of the GCC is implemented as a proportional controller for the sake of convenience. Fig. 11 shows a Bode diagram of the stability criterion $T_c(s)$ and its derivation process, when the proposed control is applied. Compared with Fig. 5, it is obvious that the closed-loop output impedance of the GCC is adjusted to be an almost resistive instead of a capacitive in load in the harmonic-frequency region, as shown in the black dash curve. This is a meaningful improvement because the original inductance-capacitance mismatch in Fig. 5 is avoided, and the peak on the amplitude-frequency curve of $T_c(s)$ is eliminated.

Fig. 12 depicts the situation where the capacitive load is switched in a microgrid. Compared with Fig. 7, the inductance-capacitance mismatch at around 400 Hz is avoided because the output impedance of the GCCs here is reconstructed to be approximately resistive. As a result, the critical peak in the amplitude-frequency curve of $T_c(s)$ in the low frequency band is eliminated. Although the other peak remains in the high frequency band, it is insignificant as previously pointed out. This proves that the proposed method based on impedance matching is effective in different situations.

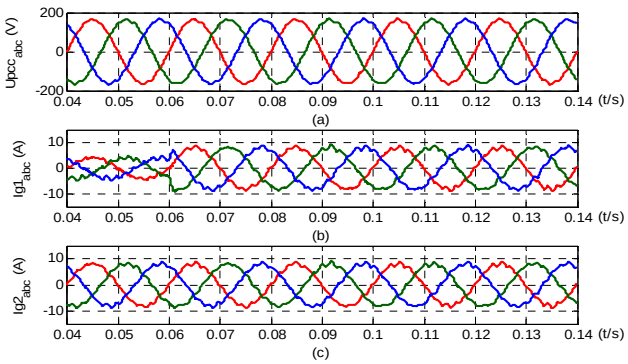

Fig. 13. Simulation by the conventional method without capacitive load.

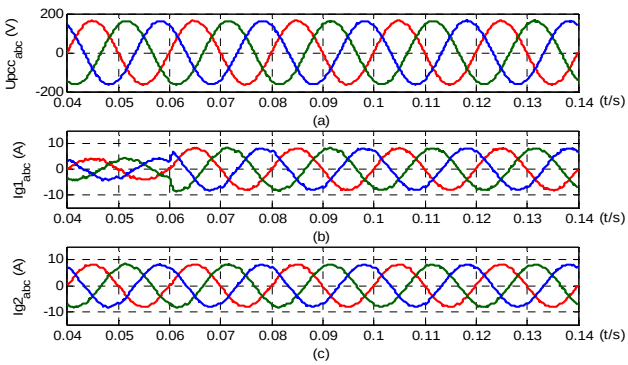

Fig. 14. Simulation by the proposed method without capacitive load.

V. SIMULATION AND EXPERIMENT VERIFICATIONS

A. Simulation Results

The configuration of the simulation system is shown in Fig. 1. There are three GCCs in the microgrid and all of the GCCs have identical circuit and control parameters. The electrical constants and control parameters are listed in Table I. The reactive current references of all the GCCs are zero. The active current references of GCC2 and GCC3 are set to 8A and the reference of GCC1 is step changed from 4 A to 8 A. Fig. 13 and Fig. 15 show the results of applying a conventional double-loop control scheme while Fig. 14 and Fig. 16 depict the situations where the proposed impedance-matching-based method is implemented. In these figures, sub-graph (a) shows the voltages of the PCC. Sub-graph (b) and sub-graph (c) show the currents of GCC1 and GCC2, respectively. The current of GCC3 is similar to GCC2 and is not displayed.

Although the capacitive loads are not switched on, as shown in Fig. 13, the measured phase currents have a certain harmonic distortion as theoretically analyzed in Fig. 5. Taking GCC2 as an example, the phase-A current is measured with a 3.5% 11^{th} harmonic distortion and a total harmonic distortion (THD) of 4.2%. This is beyond the limitation of IEEE Std 929-2000, which restricts the individual 11^{th}–15^{th} odd harmonics to within 2%. The dominating harmonic component is around 600 Hz as

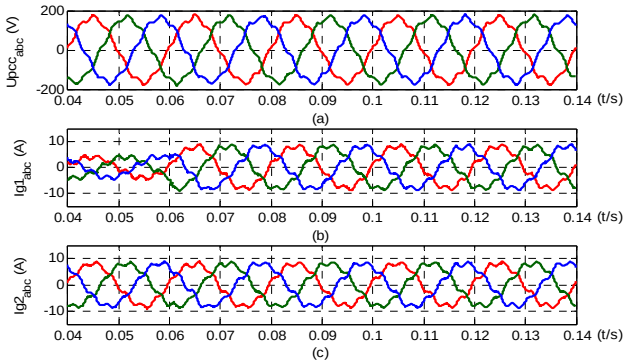

Fig. 15. Simulation by the conventional method with capacitive load.

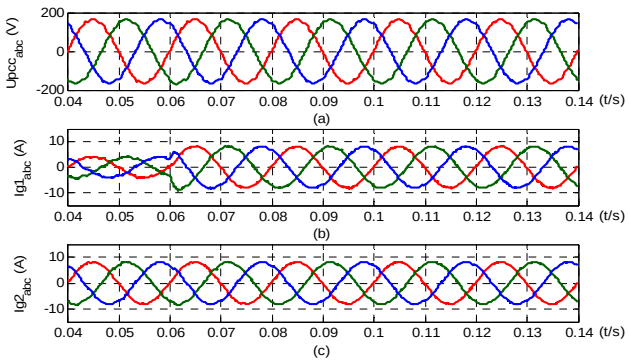

Fig. 16. Simulation by the proposed method with capacitive load.

discussed before. When the proposed method is applied, the 11th harmonic is decreased to 1.4% as shown in Fig.14, and the THD is decreased to 3.1%. As shown in Fig. 15, under the conventional control, the resonance is aggravated when a capacitive load is switched on. For this test, the THD of the current is about 7.1% with a 6.7% 7th harmonic dominating. Compared with Fig. 13, it is evident that the resonance moves to the low-frequency region, which is indicated by the stability analysis in the previous section. The improved performance with the proposed resonance damping method is shown in Fig. 16. The considerable 7th harmonic is dampened to 1.5%, and the THD decreases to 2.9%.

Considering random parameter variations and the impedance difference among the GCCs during practical operation, a simulation with a capacitive load is carried out when the filter inductances of GCC2 are increase by a further 50%, which means that the output filter impedances of the GCCs are unbalanced. Moreover, the random variations of GCC2 are undiscovered by its controller. Fig. 17 and Fig. 18 show the performances with the conventional method and the proposed method, respectively. As shown in Fig. 17, the THD of the current is about 8.4% with a 7.5% 7th harmonic dominating. Compared with Fig. 15, it is revealed that the unbalanced output filter impedances among the GCCs slightly aggravate the resonance. When the proposed method is applied, the 7th harmonic decreases to 1.4% as shown in Fig. 18, and the THD decreases to 2.9%. Another simulation

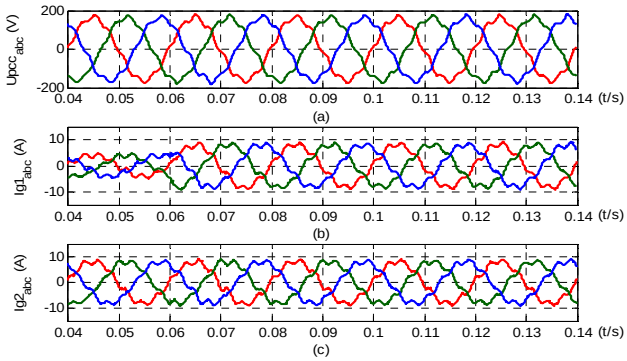

Fig. 17. Simulation with the conventional method when the output filter impedance of GCC2 increases by a further 50%.

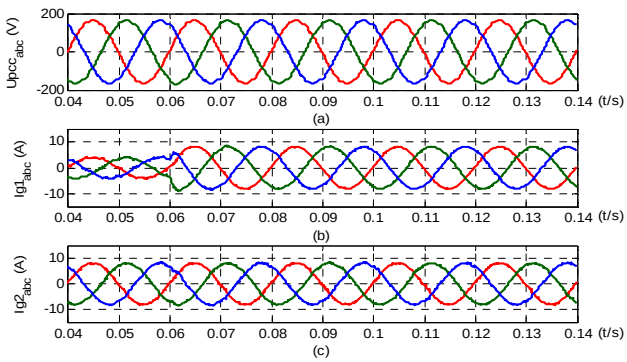

Fig. 18. Simulation with the proposed method when the output filter impedance of GCC2 increases by a further 50%.

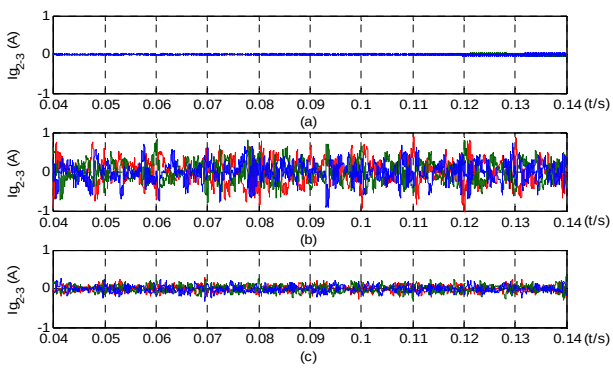

Fig. 19. Loop currents between GCC2 and GCC3 under different conditions.

is implemented when the filter inductances of GCC2 are reduced by 50%. In this case, the THD of the current is about 9.6% with an 8.5% 7th harmonic, when applying the conventional method. With the proposed method, the THD is decreased to 3.3% and the 7th harmonic decreases to 1.6%. This shows that the proposed method is immune to parameter variations in a certain range, and that it is still effective when the output filter impedances of the GCCs are unbalanced.

It is worth mentioning that harmonic loop currents among the GCCs will occur when the output filter impedances of the GCCs are unbalanced. As an example, Fig. 19 shows the loop currents between GCC2 and GCC3 under different situations.

When all of the GCCs are the same, there is almost no loop

Fig. 20. Photograph of the built experimental setup.

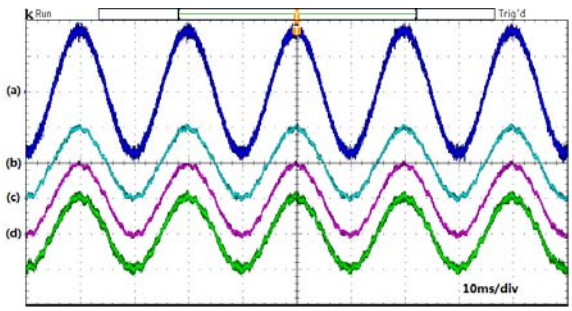

Fig. 21. Performance of the conventional method with three GCCs.

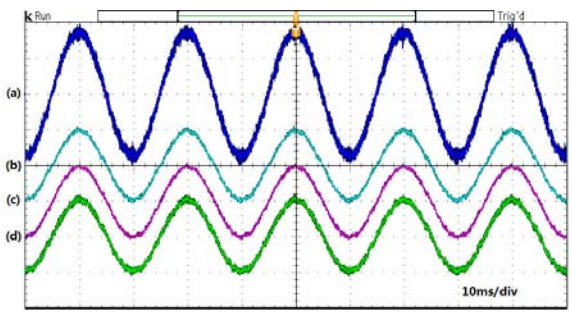

Fig. 22. Performance of the proposed method with three GCCs.

current among the GCCs, even without the proposed method, as shown in sub-graph (a). While the filter inductances of GCC2 increase by a further 50%, there are obvious loop currents between GCC2 and GCC3. They are dominated by 7th harmonic, as shown in sub-graph (b). A comparison between Fig.17 and Fig. 18 shows that with the proposed method, the harmonic resonances for all of the GCCs are well dampened. Therefore, the harmonic loop currents between GCC2 and GCC3 are attenuated, as shown in sub-graph (c). Similar results are also achieved when the filter inductances of GCC2 are reduced by 50%.

B. Experiment Results

An experimental platform based on DSP controllers is used to confirm the accuracy of the above ASM analysis, and to test the harmonic performance and practical robustness of the proposed method. Fig. 20 shows a photograph of the experimental setup in laboratory. The experimental microgrid

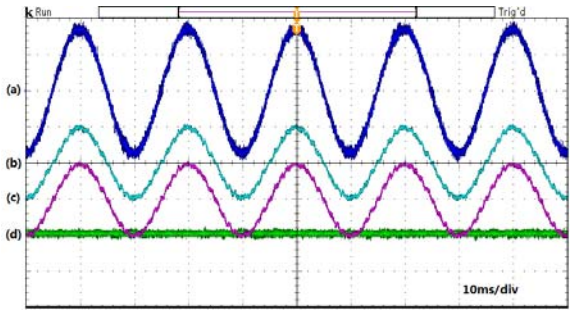

Fig. 23. Performance of the conventional method with two GCCs.

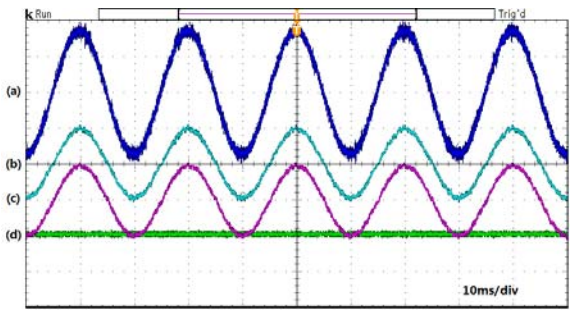

Fig. 24. Performance of the proposed method with two GCCs.

is composed of three identical GCCs, and the dc link voltages of these GCCs are provided by three-phase diode rectifiers. The relevant system settings can be found in Table I. In addition, the control algorithm is implemented on a DSP (TMS28335) plus a complex programmable logic device-based digital controller.

The performance of this microgrid consisting of three GCCs is shown in Fig. 21. This is taken as the basic case. In this figure, sub-graph (a) depicts the phase-A voltage of the PCC (100V/div). Sub-graph (b) shows the phase-A current of GCC1 (5A/div). The phase-A currents of GCC2 and GCC3 are shown in sub-graphs (c) and (d), respectively. The reactive current references for all of the GCCs are set to zero, and the active current references are set to 5A.

When the conventional control is implemented, the system is stable. However, the grid currents for all of the GCCs have an obvious steady-state resonance. For example, the phase-A current distortion of GCC1 is measured with a 5.28% THD, dominated by a 2.05% 11th harmonic and a 3.17% 13th harmonic. As depicted in Fig. 22, the proposed method reduces the THD to 3.20%. Meanwhile, the 11th harmonic decreases to 0.82% and the 13th harmonic decreases to 1.21%.

To verify the resonance frequency variation with different numbers of GCCs, GCC3 is switched out from the microgrid. In this case, there are still considerable ripples in the grid currents of the GCCs, with a 2.90% 17th harmonic and a 2.45% 19th harmonic, and the THD is 5.48%. Compared with Fig. 21, the resonance moves from 600Hz to 900Hz in Fig. 23. When the impedance-matching-based damping control is enabled, the performance of the two-GCC-based microgrid is shown in Fig. 24, where the current distortion of GCC1 has a

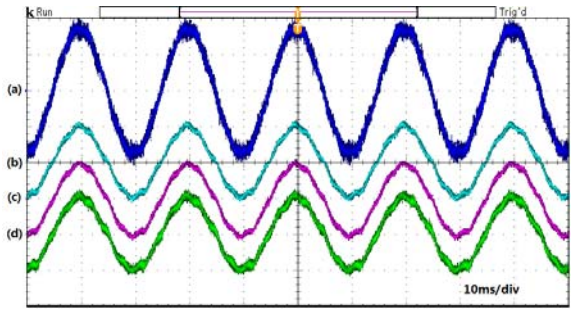

Fig. 25. Performance of the conventional method with increased grid impedance.

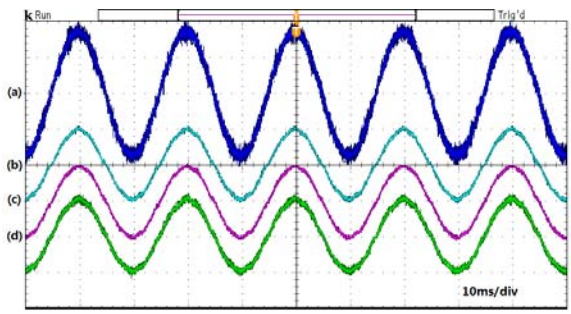

Fig. 26. Performance of the proposed method with increased grid impedance.

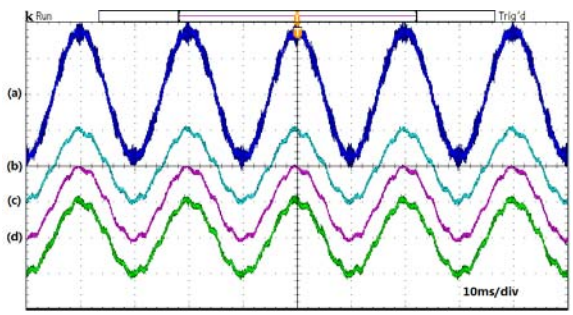

Fig. 27. Performance of the conventional method with the capacitive load.

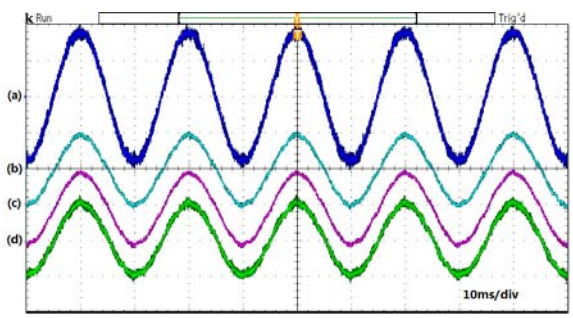

Fig. 28. Performance of the proposed method with the capacitive load.

2.83% THD. In addition, the dominating 17th and 19th harmonics decrease to 0.56% and 1.05%, respectively.

To investigate how the resonance frequency varies as the grid impedance changes, the grid inductance L_g is intentionally increased to 2.6 mH. When the conventional control is applied, the corresponding waveforms are obtained and shown in Fig. 25. Although the microgrid system remains stable, the grid currents for all of the GCCs and the PCC voltage are severely distorted. The major harmonic is the 7th harmonic, reaching up to 4.39%. Compared with the microgrid with the original grid impedance shown in Fig. 21, it is obvious that the resonance moves to the low-frequency region with an increasing grid impedance. Furthermore, it is found that this resonance can be well dampened by the proposed method. It reduces the THD from 5.62% to 3.12%, and the dominating 7th harmonic is attenuated to 1.24%.

Lastly, the capacitive load is taken into account. In this test, a capacitor is switched on in the microgrid as shown in Fig. 1. In accordance with the analysis and simulation results, the grid currents for all of the GCCs and the PCC voltage are severely distorted. Taking GCC1 as an example, the THD of the phase-A current reaches up to 6.75%, dominated by a 4.78% 7th harmonic. Compared with the basic case in Fig. 21, the aggravated resonance introduced by capacitive loads is verified. When the proposed damping scheme is adopted, the current distortion of GCC1 is measured with a 3.33% THD, and the dominant 7th also decreases form 4.78% to 1.89%. With the proposed impedance-matching-based method, the power quality of the microgrid can be significantly improved.

VI. Conclusions

The harmonic resonance and damping strategies of multiple-GCC-based microgrids have been discussed in this paper, with capacitive loads being taken into account. An impedance mismatch between GCCs and the external network in the harmonic-frequency region is found to be the primary cause of resonance in microgrids. Critical factors associated with this resonance are investigated. In addition, variations of the resonance frequency due to the number of GCCs and variations in the grid impedance are analyzed. It is also revealed that a capacitive load may aggravate the resonance. Accordingly, an impedance-matching-based control scheme is proposed to regulate the output impedance of GCCs to match it with the impedance of the external network, based on the detected resonance frequency. With this method, the resonance can be effectively suppressed in different situations.

Acknowledgment

This work is supported by National High Technology Research and Development Program of China under Grant 2015AA050606, National Key Research and Development Program under Grant 2016YFB0900302, and National Natural Science Foundation of China (NSFC) under Grant U1510208, 61273045 and 51361135705.

References

[1] F. Blaabjerg, R. Teodorescu, M. Liserre, and A. V. Timbus,

"Overview of control and grid synchronization for distributed power generation systems," *IEEE Trans. Ind. Electron.*, Vol. 53, No. 5, pp. 1398-1409, Oct. 2006.
[2] F. Wang, J. L. Duarte, and M. A. M. Hendrix, "Grid-interfacing converter systems with enhanced voltage quality for microgrid application—concept and implementation," *IEEE Trans. Power Electron.*, Vol. 26, No. 12, pp. 3501-3513, Dec. 2011.
[3] J. M. Guerrero, J. C. Vasquez, J. Matas, L.-D. Vicuna, and M. Castilla, "Hierarchical control of droop-controlled AC and DC microgrids — A general approach toward standardization," *IEEE Trans. Ind. Electron.*, Vol. 58, No. 1, pp. 158-172, Jan. 2011.
[4] J. Rocabert, A. Luna, F. Blaabjerg, and P. RodriGuez, "Control of power converters in AC microgrids," *IEEE Trans. Power Electron.*, Vol. 27,No. 11, pp. 4734-4749, Nov. 2012.
[5] W. Li, X. Ruan, D. Pan, and X. Wang, "Full-feed forward schemes of grid voltages for a three-phase LCL-type grid-connected inverter," *IEEE Trans. Ind. Electron.*, Vol. 60, No. 6, pp. 2237-2250, Jun. 2013.
[6] Z. Bai, H. Ma, D. Xu, B. Wu, and Y. Fang, "Resonance damping and harmonic suppression for grid-connected current-source converter," *IEEE Trans. Power Electron.*, Vol. 61, No. 7, pp. 3146-3154, Jul. 2014.
[7] J. He, Y. W. Li, D. Bosnjak, and B. Harris, "Investigation and active damping of multiple resonances in a parallel-inverter-based microgrid," *IEEE Trans. Power Electron.*, Vol. 28, No. 1, pp. 234-246, Jan. 2013.
[8] X. Wang, F. Blaabjerg, and W. Wu, "Modeling and analysis of harmonic stability in an AC power-electronics-based power system," *IEEE Trans. Power Electron.*, Vol. 29, No. 12, pp. 6421-6432, Dec. 2014.
[9] P. C. Loh, "Analysis of multiloop control strategies for LC/CL/LCL-filtered voltage-source and current-source inverters," *IEEE Trans. Ind. Appl.*, Vol. 41, No. 2, pp. 644-654, Mar./Apr. 2005.
[10] M. Malinowski and S. Bernet, "A simple voltage sensorless active damping scheme for three-phase PWM converters with an LCL filter," *IEEE Trans. Ind. Electron.*, Vol. 55, No. 4, pp. 1876-1880, Apr. 2008.
[11] I. J. Gabe, V. F. Montagner, and H. Pinheiro, "Design and implementation of a robust current controller for VSI connected to the grid through an LCL filter," *IEEE Trans. Power Electron.*, Vol. 24, No. 6, pp. 1444-1452, Jun. 2009.
[12] G. Shen, D. Xu, L. Cao, and X. Zhu, "An improved control strategy for grid-connected voltage source inverters with an LCL filter," *IEEE Trans. Power Electron.*, Vol. 23, No. 4, pp. 1899-1906, Jul. 2008.
[13] J. Dannehl, F. W. Fuchs, S. Hansen, and P. B. Thogersen, "Investigation of active damping approaches for PI-based current control of grid-connected pulse width modulation converters with LCL filters," *IEEE Trans. Ind. Appl.*, Vol. 46, No. 4, pp. 1509-1517, Jul./Aug. 2010.
[14] F. Liu, Y. Zhou, S. Duan, J. Yin, and B. Liu, "Parameter design of a two-current-loop controller used in a grid-connected inverter system with LCL filter," *IEEE Trans. Ind. Electron.*, Vol. 56, No. 11, pp. 4483-4491, Nov. 2009.
[15] J. He, and Y. W. Li, "Generalized closed-loop control schemes with embedded virtual impedances for voltage source converters with LC or LCL filters," *IEEE Trans. Power Electron.*, Vol. 27, No. 4, pp. 1850-1861, Apr. 2012.
[16] C. Bao, X. Ruan, X. Wang, W. Li, and D. Pan, "Step-by-step controller design for LCL-type grid-connected inverter with capacitor current-feedback active-damping," *IEEE Trans. Power Electron.*, Vol. 29, No. 3, pp. 1239-1253, Mar. 2014.
[17] J. Dannehl, F. W. Fuchs, and P. B. Thogersen, "PI state space current control of grid-connected PWM converters with LCL filters," *IEEE Trans. Power Electron.*, Vol. 25, No. 9, pp. 2320-2330, Sep. 2010.
[18] S. G. Parker, B. P. Mcgrath, and D. G. Holmes, "A general discrete time model to evaluate active damping of grid converters with LCL filters," in *Proc. ECCE-ASIA*, pp. 2019-2026, 2014.
[19] J. L. Agorreta, M. Borrega, J. Lopez, and L. Marroyo, "Modelling and control of N paralleled grid-connected inverters with LCL filter coupled due to grid impedance in PV plants," *IEEE Trans. Power Electron.*, Vol. 26, No. 3, pp. 770-785, May 2011.
[20] J. H. R. Enslin, and P. J. M. Heskes, "Harmonic interaction between a large number of distributed power inverters and the distribution network," *IEEE Trans. Power Electron.*, Vol. 19, No. 6, pp. 1586-1593, Nov. 2004.
[21] X. Wang, F. Blaabjerg, M. Liserre, and Z. Chen, "An active damper for stabilizing power-electronics-based AC systems," *IEEE Trans. Power Electron.*, Vol. 29, No. 7, pp. 3318-3329, Jul. 2014.
[22] X. Sun, L. Yang, R. Wang, and R. Han, "A Novel Impedance Converter for Harmonic Damping in Loop Power Distribution Systems," *IEEE Journal of Emerging and Selected Topics in Power Electronics*, Vol. 4, No. 1, pp. 162-173, Mar. 2016.
[23] J. Sun, "Small-signal methods for AC distributed power systems — A review," *IEEE Trans. Power Electron.*, Vol. 24, No. 12, pp. 2545-2554, Dec. 2009.
[24] S. Zhang, S. Jiang, X. Lu, B. Ge, and F. Z. Peng, "Resonance issues and damping techniques for grid-connected inverters with long transmission cable," *IEEE Trans. Power Electron.*, Vol. 29, No. 1, pp. 110-120, Jan. 2014.
[25] E. Twining, and D. G. Holmes, "Grid current regulation of a three-phase voltage source inverter with an LCL input filter," *IEEE Trans. Power Electron.*, Vol. 18, No. 3, pp. 888-895, May 2003.
[26] J. Sun, "Impedance-based stability criterion for grid-connected converters," *IEEE Trans. Power Electron.*, Vol. 26, No. 11, pp. 3075-3078, Nov.2011.

Shulong Tan was born in Hunan, China. He received his B.S. degree in Automation from the Huazhong University of Science and Technology, Wuhan, China, in 2012. He is presently working towards his Ph.D. degree at Tsinghua University, Beijing, China. He is also working as a Research Assistant in the Department of Automation, Tsinghua University. His current research interests include the stability problems of inverter-based renewable power generation systems.

Hua Geng was born in Jiangsu, China. He received his B.S. degree in Electrical Engineering from the Huazhong University of Science and Technology, Wuhan, China, in 2003; and his Ph.D. degree in Control Theory and Application from Tsinghua University, Beijing, China, in 2008. From 2008 to 2010, he was a Postdoctoral Research Fellow in the Department of Electrical and Computer Engineering, Ryerson University, Toronto, ON, Canada. Since May 2010, he has been an Assistant Professor in the Department of Automation, Tsinghua University. His current research interests include distribution generation systems, renewable energy conversion systems, and digital control systems. He is an Associate Editor for the IEEE Transaction on Industry Applications and the IEEE Transaction on Energy Conversion.

Geng Yang was born in Ningxia, China. He received his B.S. and M.S. degrees in Electrical Engineering from the Xi'an University of Science and Technology, Xi'an, China, in 1982 and 1984, respectively; and his Ph.D. degree in Electrical Engineering from Sophia University, Chiyoda, Japan, in 1992. From 1985 to 1987, he was an Assistant at the Xi'an University of Science and Technology. He was a Visiting Scientist with Fukui State University, Fukui, Japan, in 1987; and with Sophia University, Tokyo, Japan, in 1988. From 1992 to 1994, he was a Senior Researcher with Kasuga Electrical Works Ltd., Mitaka, Japan. From 1995 to 1999, he was a Lecturer, Associate Professor, and Professor with the Xi'an University of Science and Technology. Since 2000, he has been a Professor in the Department of Automation, Tsinghua University, Beijing, China. His current research interests include electrical drives and systems, power electronic equipment, and the control technology of wind and photovoltaic energy conversion systems. Dr. Yang is a member of the Institute of Electrical Engineers of Japan and the Board Directors of the China Power Electric Institute. He is a member of the China Electrotechnical Society (CES) and serves as the Vice-Director of the Education Committee of the Electrical Automation Branch in CES.